Journal of Structural Geology, Vol. 10, No. 8, pp. 779 to 793, 1988
Printed in Great Britain

0191-8141/88 $03.00 + 0.00

Simulation of fabric development in recrystallizing aggregates—II. Example model runs

M. W. JESSELL

Department of Geological Sciences, State University of New York at Albany, Albany, NY 12222, U.S.A.*

(*Received* 30 *August* 1987; *accepted in revised form* 20 *June* 1988)

Abstract—This study investigates the role of the coupling of dynamic recrystallization and lattice rotations in fabric development. A new two-dimensional computer simulation of polycrystalline deformation is used, which combines homogeneous straining, internal lattice rotations and dynamic recrystallization processes. Five example runs of the simulation are described here, which compare the progressive development of fabrics resulting from different recrystallization regimes and different straining geometries. It is found that these fabrics can evolve significantly with progressive strain from one strong fabric pattern to another. The effect of recrystallization is not only to create point maxima concentrations of *c*-axes, but also to modify and create girdle distributions. Correlations are made between the fabrics generated by this model and previously reported quartz and ice fabrics.

INTRODUCTION

CURRENT models of crystallographic fabric development are based on the lattice rotations induced by crystal slip (Etchecopar 1977, Lister *et al.* 1978) and these models are able to account for some of the characteristics of observed fabrics in naturally and experimentally deformed rocks. The role of recrystallization in fabric development has been recognized to be important (Kamb 1972, Duval 1981, Bouchez *et al.* 1983, Urai *et al.* 1986), however the relative importance of these two processes has been uncertain. In order to investigate their interaction, a simulation of fabric evolution in recrystallizing aggregates has been developed (Jessell 1988). In this paper five runs of this simulation are presented which demonstrate the diversity of fabrics that may result from different deformation geometries and recrystallization regimes.

MODEL DESCRIPTION

The basis for this model, which is described in Jessell (1988), is a two-dimensional triangular array of points. Each of the 10,000 points in this array represents a small area of material, and is assigned a *c*-axis orientation at the start of the simulation. Point clusters with the same orientation define the extent of individual grains.

The model simulates polycrystalline deformation in materials with hexagonal symmetry by repeatedly applying approximations to four syn-deformational processes. A single iteration of the simulation consists of (1) the redistribution of points to approximate homogeneous straining; (2) reorientation of the *c*-axes associated with each point to approximate the lattice rotations for quartz predicted by Taylor–Bishop–Hill theory (Lister *et al.* 1978); (3) switching of orientations at grain boundaries to simulate grain boundary migration; and (4) the nucleation of subgrains.

The driving force for grain boundary migration is assumed to be the stored energy of deformation, which in turn is assumed to be crystallographically controlled, as postulated by Duval (1981), Urai & Humphreys (1981), Jessell (1986) and Schmid & Casey (1986). Grains which have their active crystal slip systems parallel to the orientation of the planes of maximum resolved shear stress, and can be easily activated by the shear couple, will accumulate low levels of stored energy. It is also assumed that the levels of stored energy are related to the finite strain undergone by a grain.

The model starts off with 300 grains, each made up of 37 points (of unit area), except for the ones truncated by boundaries, and each grain is randomly assigned a *c*-axis orientation. In the simple shear runs, grains that are shifted by the straining beyond the vertical boundary to the left reappear on the right-hand side, since this reduces any boundary effects.

In the descriptions which follow the orientations of the maximum and minimum stress axes are assumed to be parallel to the bounds of the array in axisymmetric flattening, and at 45° to them in simple shear. The model produces grain boundary maps and *c*-axis fabric diagrams after each iteration, so that the progressive development of the fabric can be followed. The parameters controlling the evolution of the five runs are compared in Table 1.

EXAMPLE MODEL RUNS

Run 1

In this run, which serves as the control against which the other four can be compared, the stored energy of

*Present address: Department of Earth Sciences, Monash University, Clayton, Victoria, 3168, Australia.

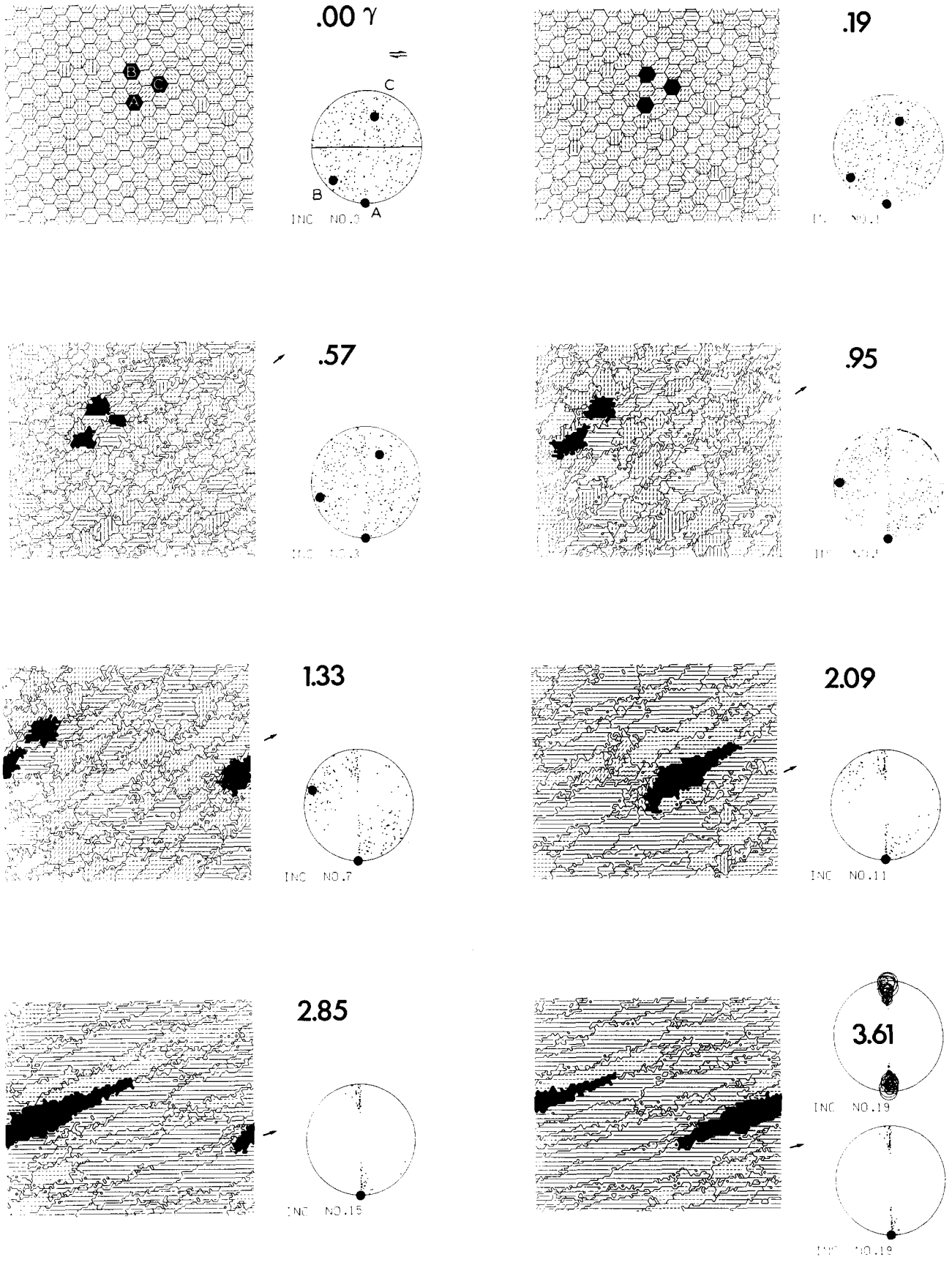

Fig. 1. Run 1: grain boundary maps and lower-hemisphere equal-area *c*-axis projections. The deformation geometry is dextral simple shear, with stored energy patterns controlled by basal ⟨*a*⟩ slip systems, a mobility of 1 and no subgrain formation. See text for detailed discussion. For each element of the figure the large number shows the finite shear strain, the single arrow shows the orientation of λ_1, and the shaded areas are reference grains. The number of increments is also indicated. The short strokes within grains are parallel to the basal plane trace and have lengths proportional to basal plane dips out of the plane of the diagram.

Table 1. Comparison of the parameters used in the simulation runs described in this paper

	Run 1	Run 2	Run 3	Run 4	Run 5
Deformation geometry	SS*	SS	SS	SS	ASF
Lattice rotation rate (maximum)	10°	10°	10°	10°	5°
Strain per increment	0.19γ	0.19γ	0.19γ	0.19γ	9%
Stored energy control	Basal ⟨a⟩	Prism ⟨a⟩	Basal ⟨a⟩	Basal ⟨a⟩	Basal ⟨a⟩
Grain boundary mobility	5	5	5	0.5	5
Nucleation type	None	None	±10°	None	None
Nucleation rate	0	0	0.0025	0	0
Fig. No.	1	3	4	6	7

*SS: simple shear; ASF: axisymmetric flattening.

deformation is defined as being controlled by the orientations of the basal planes of the grains, and no subgrains are formed. The deformation geometry is progressive dextral simple shear, with each increment of shear set to 0.19. The evolution of the grain shape and *c*-axis fabrics is shown in Fig. 1, starting with the initial fabrics.

Shear strain = 0.0. The starting configuration consists of hexagonally-shaped grains with random *c*-axis orientations. The grain boundaries are drawn as a connected network of lines, and the individual grain orientations are shown by the strokes within grains. The strokes are parallel to the basal plane traces for each grain and the lengths of the strokes are proportional to basal plane dips away from the depicted plane, with longer strokes representing steeper dips. The orientation of λ_1 is also shown for each stage as an arrow pointing away from the lower left-hand corner of the area. A simple comparison between the orientation of the grain shape foliation and λ_1 can be made by aligning a ruler with the lower left-hand corner and the arrow. The shear plane is horizontal, and the top row is a fixed material line. Three grains have been labeled so that their histories may be followed and compared. Lower-hemisphere equal-area projections of the *c*-axes at equivalent strains to the grain boundary maps are also shown, together with the orientation of the shear plane and the three reference grains. The number beneath each *c*-axis diagram shows the increment number.

Shear strain = 0.19. Apart from the change in shape due to the straining, there are no significant departures from the initial fabric. The strain has displaced the lower grains to the left so that the line of edge grains now slopes down from the top right corner. No grain boundary migration has taken place since the model assumes no stored energy build up during the first increment of deformation of a grain. The small variations in grain geometry are due to the approximation to homogeneous strain used in this model.

Shear strain = 0.57. The stored energy of grains, which is partially a function of grain age, is now high and variable enough to drive grain boundary migration. Hence many grains that have orientations such that they lead to high levels of stored energy have been consumed or dissected by their neighbours, producing many grains which have a grain size of one. Grain C, at present relatively poorly oriented for slip on its basal plane, has shrunk slightly. In contrast, both grains A and B are larger than their initial sizes. The large number of dissected grains, forming the 'left over grains' of Urai (1983), result in an average grain area of 25 units (calculated by dividing the number of grains into 10,000), which is smaller than the starting size of 37 units. Figure 2 is a graph of average grain size vs strain for all the example simulations. A weakly defined grain shape fabric has developed, which may lag slightly behind λ_1. No obvious changes in the *c*-axis fabric are evident.

Shear strain = 0.95. The average grain size at this strain is 27 units, however this masks a considerable amount of grain growth. A bimodal grain size distribution has developed, with many grains being 2–3 times their starting size, and most of the rest close to a grain size of 1 unit. Grains A and B continued their growth, and grain C has been totally consumed. The basal traces are mostly either subparallel or subperpendicular to the shear plane, however the *c*-axis fabric diagram shows that many of the smaller grains (whose basal traces do not show up on the fabric map) have other orientations, as the fabric is still diffuse. Grain A has maintained its initial orientation, since the lattice reorientation patterns predict that its *c*-axis is stable in this orientation.

Shear strain = 1.33. The growth rates of grains A and B are now diverging, with grain A continuing to grow, but grain B, which has a basal plane which is now

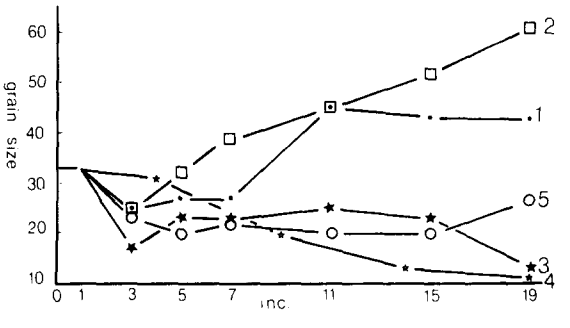

Fig. 2. Evolution of average grain areas (calculated by dividing the number of grains into 10,000) with incremental deformation for the five example runs. The axisymmetric flattening curve (Run 5) is normalized to account for area loss.

rotating away from an orientation of minimum stored energy, shows little further growth. As a result of the reduction in the range of the remaining *c*-axis orientations, many neighbouring grains now have very similar orientations, so that subgrain boundaries, rather than grain boundaries, now separate them. Thus even though a clear grain shape fabric exists in terms of original grain boundaries, grain coalescence may effectively mask it. The equilibrium between the number of consumed and dissected grains has kept the grain size at 27 units. The *c*-axis fabric shows an incomplete girdle perpendicular to the flow direction, but there is still a large scatter of orientations. The grain shape foliation continues to lag slightly behind λ_1, so that although it does not quite track the accumulation of finite strain, it is not stable either.

Shear strain = 2.09. In the intervening period grain B has been totally consumed. Its rapid demise is explained by its basal plane becoming parallel to σ_3, a maximum stored-energy orientation. Grain A is now more or less surrounded by similarly oriented grains, and thus the driving force for grain boundary migration is low. Many of the remaining 'poorly' oriented grains have been consumed, increasing the mean grain size to 45, the first time it has been larger than the starting value, although using mean grain sizes severely underestimates the extent of grain growth associated with the deformation. The grain shape foliation now roughly parallels λ_1, although in reality there are nearly as many subgrain as grain boundaries now. The *c*-axis pattern now consists of a severely interrupted girdle, or an elongate point maximum, together with an asymmetric tail.

Shear strain = 2.85. Many of the *c*-axes away from the point maximum disappeared during this interval, and the whole area now consists of a near single-crystal fabric, with little likelihood of change, since the grains are in stable lattice orientations and the differential stored energy between grains is low.

Shear strain = 3.61. The grain size has more or less stabilized at 45 units, and the grain shape foliation continues to track λ_1. The predicted axial ratio of grains that have undergone this strain is 8.5:1. This is close to the measured ratio of 7.8:1 (grain A has an axial ratio of 9:1). The measured axial ratio only includes the 10 largest grains, as the shape of these grains is least dependent on the triangular nature of the array, and many others are truncated by the horizontal boundaries of the model. Again these measurements ignore grain coalescences by grain boundary migration or lattice rotations. Including the smaller grains would reduce the mean axial ratio. The *c*-axis fabric still shows something intermediate between a point maximum and an interrupted girdle; however if the fabric is plotted with circles proportional to grain areas, the pattern closely resembles a point maximum, and any further deformation would sharpen this distinction.

Run 2

This run only differs from Run 1 in the imposed pattern of the stored energy of deformation, now controlled by the prism $\langle a \rangle$ slip systems. The grain shape fabric maps are shown in Fig. 3, together with the *c*-axis projections. Here, two grains are sufficient to demonstrate the typical grain histories, as the grains display less variation, tending either to grow or shrink monotonously. This simple behaviour results from the shared symmetry of the stored energy distribution and the lattice rotations, so that grains never rotate away from the levels of stored energy they start with. This is in contrast to Run 1, where grains were free to rotate in and out of stored energy maxima and minima. The two highlighted grains have similar basal plane trace orientations, however grain A has a shallower basal plane dip.

Shear strain = 0.0–0.95. Fabric evolution observed in the first five increments of this run is virtually indistinguishable from that in Run 1. Here there is a slight depopulation of grains with steep basal plane dips, which shows up as a preponderance of shorter basal traces in these maps; however this contrast is much less pronounced in the *c*-axis projections. At $\gamma = 0.95$ the growth of grain A has resulted in a complex grain geometry, although the grain shape fabric as a whole is well developed, and parallels λ_1; in contrast three 'left over grains' (Urai 1983) have resulted from the partial consumption of grain B. By $\gamma = 0.95$ the number of consumed grains has been almost exactly compensated for by the number of dissected grains, so that the grain size, after an initial decrease, is back to its starting value. As in the first run, a bimodal grain size distribution has formed. From the grain shape alone no evidence of the starting grain size remains, so that the resulting fabric could be interpreted as having formed from the deformation of a polycrystal of this grain size together with a minor amount of nucleation of new grains at grain boundaries.

Shear strain = 1.33. Clear variations between this run and Run 1 are now evident, in both the *c*-axis and grain shape fabrics. The individual grains in this run are larger, and there are fewer of the unit-sized remnant grains. The reason for this is the relatively simple growth history of these grains, which in turn is due to shared symmetry of the lattice rotation patterns and the stored energy patterns. Grain A has continued to grow, and grain B (labeled) is now reduced to a single unit-sized remnant. The *c*-axis distribution is now beginning to show two maxima. This develops because of the selective consumption of grains with steep basal plane dips, coupled with the initial low number of grains with very shallow basal plane dips (in any uniform distribution of orientations in space, to which a random *c*-axis fabric approximates, there is a sinusoidal frequency distribution of orientations away from any given direction).

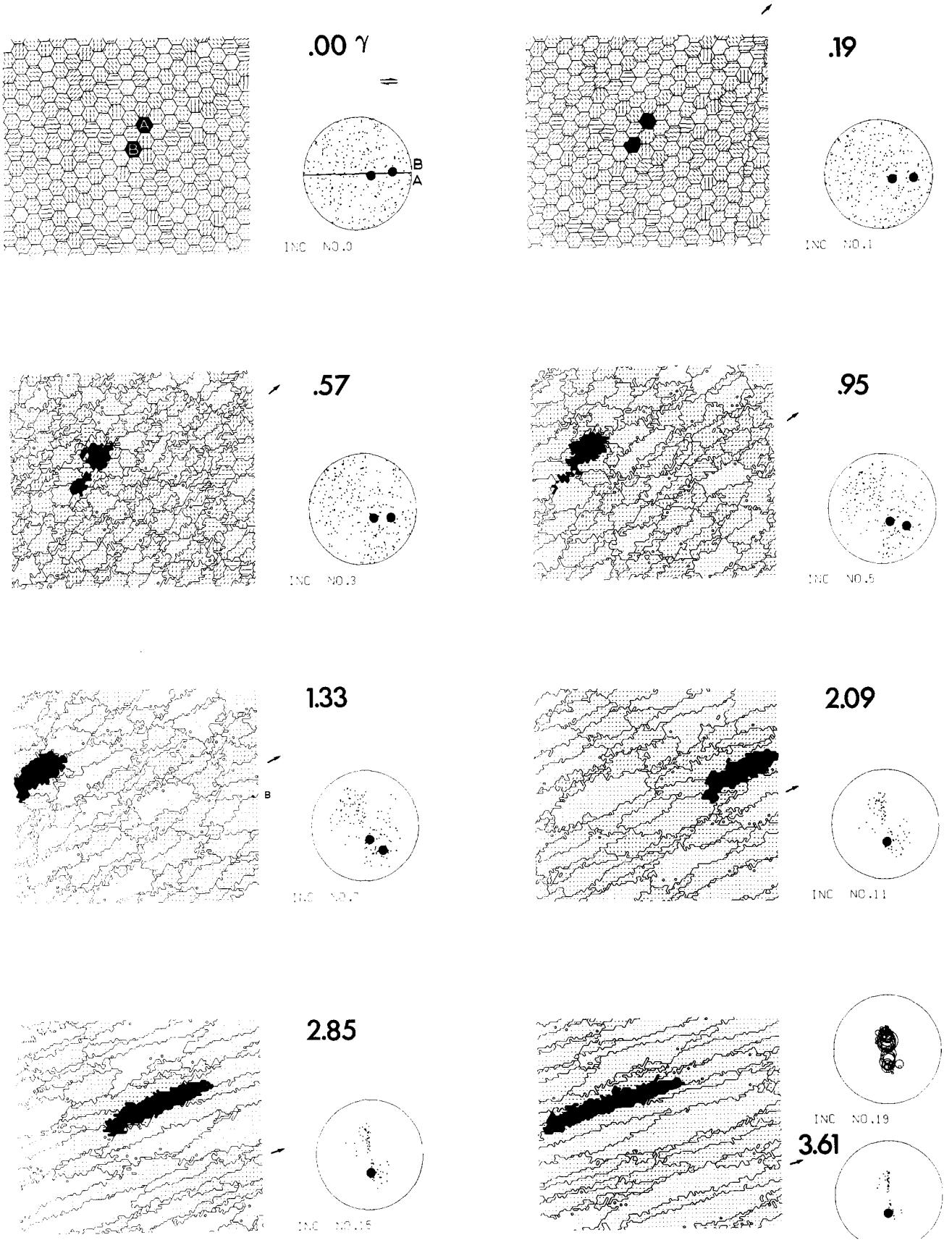

Fig. 3. Run 2: all parameters and details of the figure are as for Run 1, except that the stored energy of deformation is controlled by prism ⟨*a*⟩ slip.

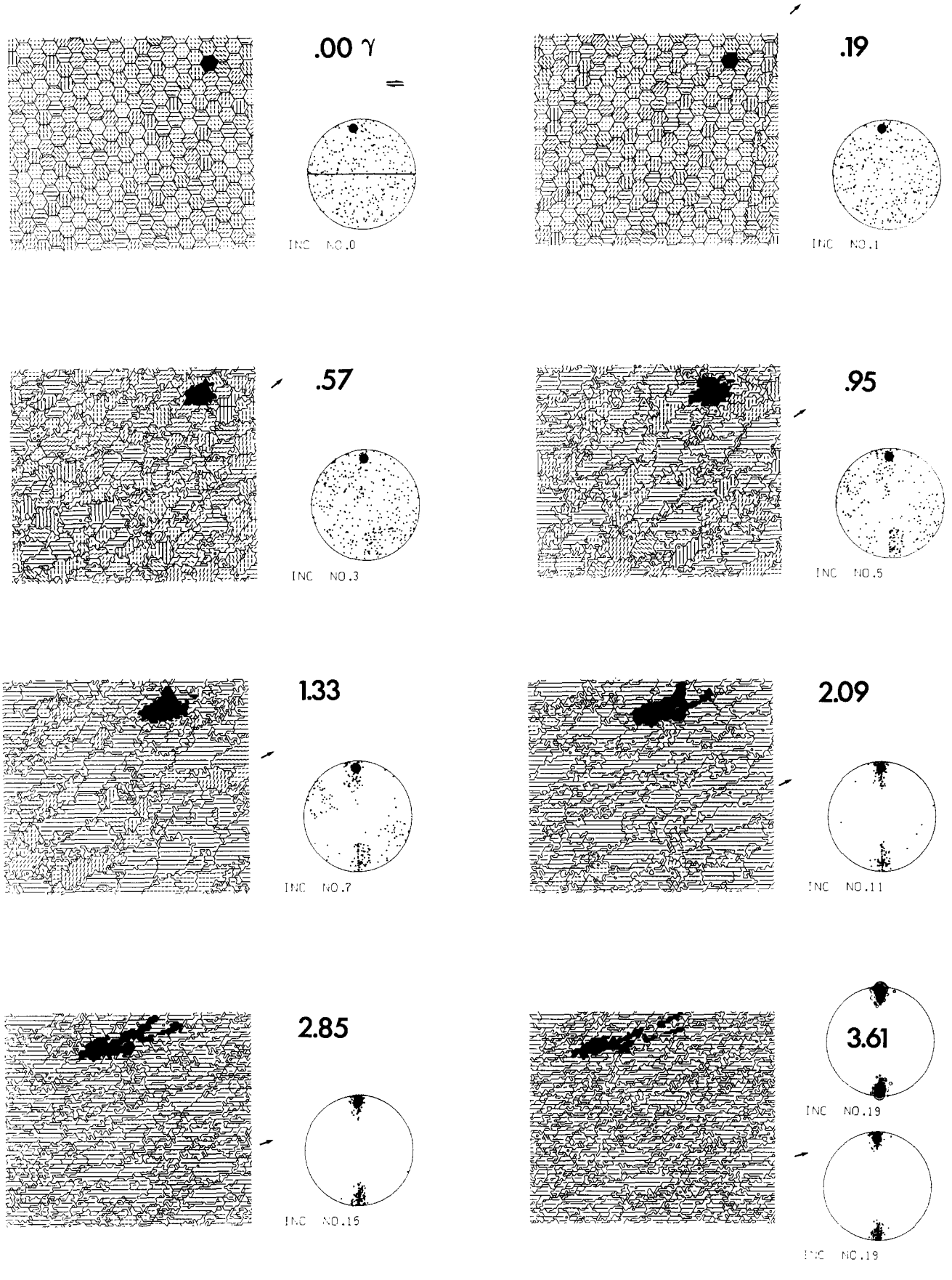

Fig. 4. Run 3: all parameters and details of the figure are as for Run 1, except that the nucleation of subgrains is allowed.

Shear strain = 2.09. A strong two-maxima *c*-axis pattern has now developed, with the maxima lying on a great circle which is roughly perpendicular to the orientation of maximum finite elongation. Grains with steep basal plane dips are still being progressively removed, so that the positions of the point maxima migrate towards the λ_2 direction.

Shear strain = 2.85–3.61. As in Run 1 the much reduced range of lattice orientations results in a sharp decrease in the driving force for grain boundary migration, although grain growth continues (up to 61 units), as a result of the consumption of small grains. Hence the main control on grain shape is now the continued straining. The two point maxima continue to sharpen, and are now close to the λ_2 direction. A plot of grain size vs orientation shows that the pattern is in essence a single maximum, elongate perpendicular to the flow plane. Continued deformation would sharpen this single maximum further, but would not greatly change its character.

Run 3

In this run, as in Run 1, the stored energy of deformation is controlled by the orientation of the basal ⟨*a*⟩ slip systems, and it also shares the same grain boundary mobility; however in this run the fabric is also modified by the nucleation of strain free subgrains. These subgrains are constrained to form with *c*-axis orientations within 10° of the *c*-axis orientation of the host grain. This rather crude algorithm is meant to represent rotation recrystallization. The development of the grain shape and crystallographic fabrics is shown in Fig. 4.

Shear strain = 0.0–0.19. The process of subgrain formation does not start until a minimum stored-energy level is reached within the host grain, so the evolution up to this stage is essentially identical to that of Run 1.

Shear strain = 0.57. Nucleation of new subgrains has now commenced, resulting in a weaker grain shape fabric than seen in Run 1, and a smaller average grain size (17 units), although if applied to a real polycrystal, these statements would only apply if the misorientation between host grain and subgrain was sufficiently large that they could be considered to be separate grains.

Shear strain = 0.95. In this run, as in Run 1, the grain size has increased, in this case to 23 units, as dissected grains which reduce the average grain size are totally consumed. Subgrain formation has started to have an effect on grain shapes, since even the well-oriented example grain has started to become dissected. The bimodal grain size is less apparent in this run, as the subgrains (which initially grow because of their low stored energy levels) fill in the gap in grain sizes. The *c*-axis fabrics are also beginning to differ significantly, with a clearer concentration of *c*-axes perpendicular to the flow plane.

Shear strain = 1.33. The mean grain size is still 23 units, suggesting an equilibrium between subgrain formation and dissection and consumption of grains, although again the grain size of all but the smallest fraction is still increasing. The *c*-axis fabric has developed into a strong maximum perpendicular to the flow plane, with a weaker secondary maximum about 60° away from the first maximum. As in Run 2, the *c*-axis fabric has a rough symmetry across the grain shape foliation plane, the main asymmetry coming from the unequally populated maxima.

Shear strain = 2.09. Continued subgrain formation and growth has produced very irregular grain shapes, many grains having multiple lobes. The *c*-axis fabric is now a single point maximum, the grains in the other maximum having either been rotated out of this orientation or consumed by their neighbours. The sharp single maximum has thus developed earlier than in Run 1.

Shear strain = 2.85–3.61. Although there are still many large grains, they have complex geometries, and the grain size has dropped to 13 units. The average grain elongation orientation lags about 15° behind λ_1 (see Fig. 5). The histogram in Fig. 5 was constructed by measuring the orientation of the long axes of the largest 237 grains. The smaller grains were ignored because their shape is dependent on the triangular geometry of the base array. The very largest fraction of grains do in fact lie parallel to λ_1, and it is the more numerous intermediate-sized grains which produce the oblique foliation. Even by a shear strain of 3.61 this run has clearly not reached a stable grain shape configuration, and simulations to higher strains would be of interest.

Run 4

In this run the effects of a 10-fold reduction in the mobility of grain boundaries are investigated, all other parameters having the same values as in Run 1. Since the

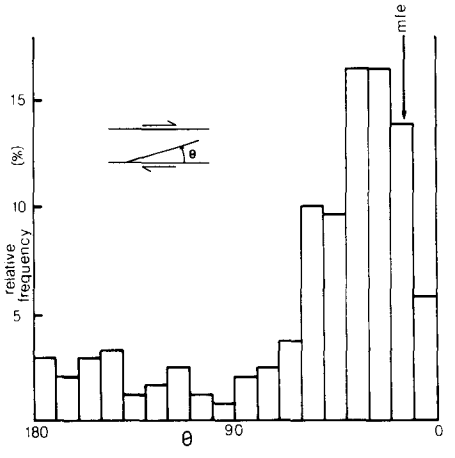

Fig. 5. Relative frequency histogram of grain elongation orientations for γ = 3.61, Run 3 (the largest 237 grains). The maximum lags about 15° behind λ_1 (the position of which is shown by mfe).

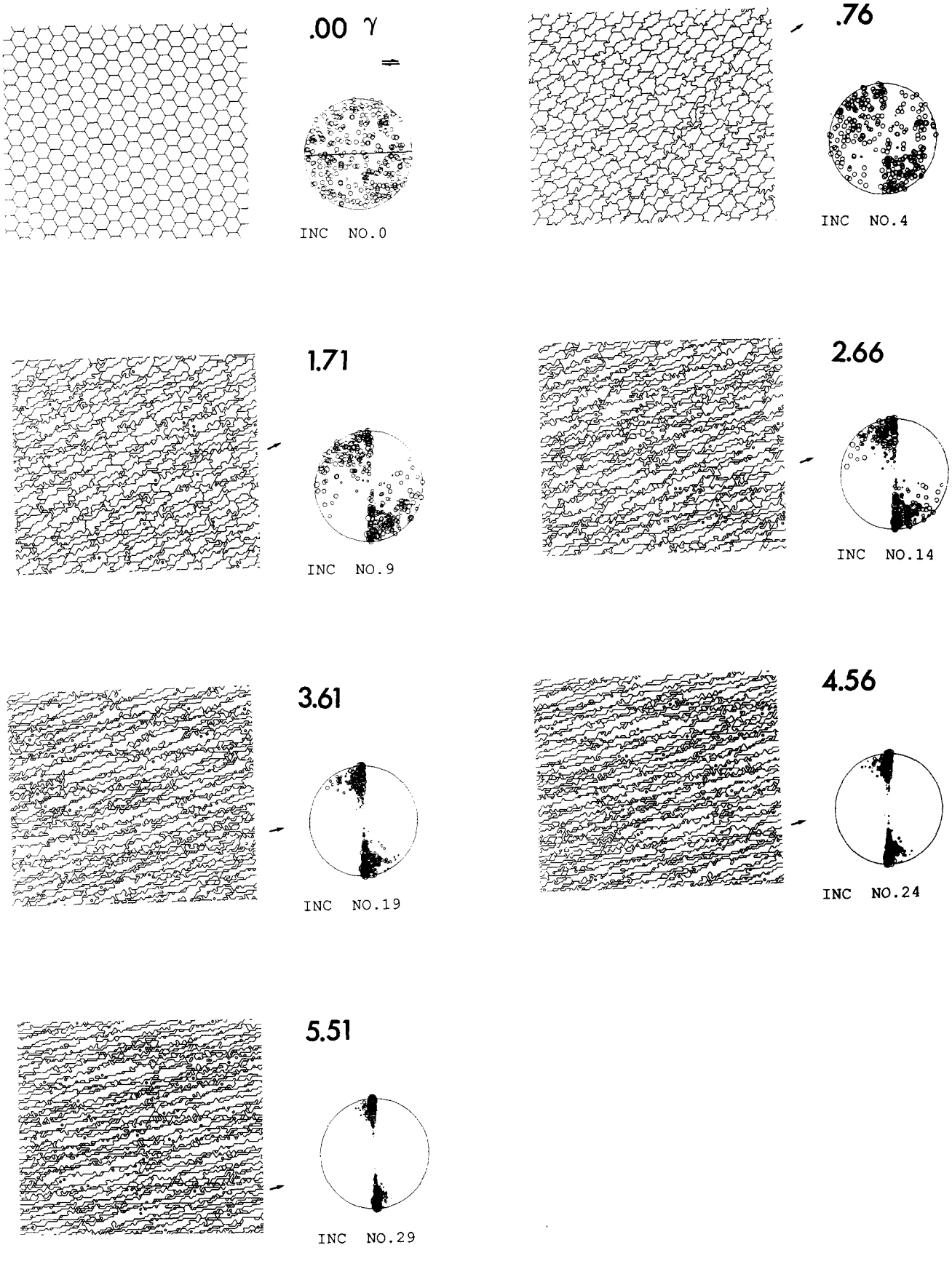

Fig. 6. Run 4: all parameters and details of the figure are as for Run 1, except that the mobility of all grain boundaries is lowered by an order of magnitude, basal plane traces are not shown, and plots of grain size vs orientation of *c*-axes are given. Note also that higher finite strains are reached in this run.

effects of recrystallization are slowed by the lower mobility, this run was extended to 29 increments, instead of the usual 19. Two further changes were made to the method of depiction of fabrics to help clarify its evolution: only grain boundaries are shown in the grain boundary maps, and grain size vs orientation diagrams are used (Fig. 6).

Shear strain = 0.0–1.71. As might be expected for such low grain boundary mobilities, the grain shape and crystallographic fabrics that develop at low strains are virtually indistinguishable from the fabrics that form without recrystallization. In addition the variations in grain size with orientation are almost imperceptible. A Type I cross-girdle of *c*-axes has formed; however there are still many off-girdle orientations. Due to the low grain-boundary velocities the grain size does not drop as rapidly during the first increments, however it does slowly decline so that by a shear strain of 1.71 it is less than half of the grain size in Run 1 at the same strain.

Shear strain = 2.66–3.61. The cross-girdle *c*-axis pattern has sharpened further, and the grain shape fabric continues to give a remarkably 'unrecrystallized' appearance.

Shear strain = 4.56–5.51. The *c*-axis fabric has now changed from the cross-girdle pattern, as a result of the selective consumption of grains away from the plane perpendicular to the flow direction. These grains are preferentially consumed because they lie in higher stored strain energy orientations. The flow-plane normal girdle is also modified, with *c*-axes at a low angle to the shear plane having been removed; further deformation would clearly have led to a contraction of the fabric towards a point maximum. The grain-shape fabric continues to track λ_1, and the grain size is slowly dropping, although at a decelerating rate (Fig. 2).

Run 5

The fifth example run is intended to be the equivalent of Run 1, except that the deformation geometry is axially-symmetric flattening. The stored energy is again controlled by the orientation of the basal plane. As discussed in Jessell (1988), the use of different principles to simulate the two deformation geometries introduces an unwanted complication when comparing the fabrics, since they lead to different amounts of disruption of the grain-shape fabric; furthermore axisymmetric flattening removes material from the plane of interest. In order to avoid these complications, simulations were also carried out with the strain algorithms removed, and only the recrystallization and lattice rotation algorithms activated. Results from the 'unstrained' runs confirm the observations highlighted below. The simulation run with the strain algorithm activated is shown in Fig. 7. In this run reported grain sizes are normalized for area loss.

Shortening = 0–25%. As might be expected, the major differences in fabric development are the direct result of deformation geometry. Grains have become preferentially elongate perpendicular to the shortening direction, and the *c*-axis fabric is characterized by a pole-free region which forms a girdle perpendicular to the shortening direction.

Shortening = 40–49%. The grain-shape fabric has strengthened, however the size of the largest grain-size fraction is much smaller than that formed in Run 1. When the grain size is normalized for area loss, it still only reaches 22 units. The *c*-axis fabric has started to develop a pole-free area parallel to σ_1, a maximum stored-energy orientation. Combined with the pole-free girdle perpendicular to σ_1, this produces a small circle girdle.

Shortening = 65–83%. The evolution of the grain-shape fabric is still slow, the expected axial ratio by the end of the run would be 15.4:1, whereas the axial ratio of even the 10 largest grains is only 3.6:1. The final normalized grain size is 27 units, far below the grain size in comparable simple shear runs. The *c*-axis girdle tightens slowly, due to the rotation of grains towards σ_1 on the outside of the girdle, and the consumption of grains on the inside. Once a fairly tight girdle has formed, most of the driving force for grain boundary migration is removed, and further deformation results in the closure of the girdle towards σ_1.

DISCUSSION

c-axis fabrics

As one end-member, without dynamic recrystallization, these simulations mimic the formation of fabrics predicted by the Taylor–Bishop–Hill (TBH) analysis. Price (1985) has compared natural quartzite fabrics with those predicted by TBH theory for similar strains, and concluded that "many of the observed patterns of preferred *c*-axis orientation agree with predicted patterns at similar strains". Of interest here are the fabrics that deviate from these predictions. Even though this model strictly only applies to the deformation of quartzites, analogies will be drawn with fabric development in ice, since the lattice rotations are sufficiently removed from the original TBH predictions that arguably they may also apply to the more general case of deformation of a polycrystal with hexagonal symmetry.

Point maxima fabrics

Wilson (1973) has measured a number of *c*-axis fabrics adjacent to the Mt Isa Fault in Australia, and many of these fabrics resemble the shear-plane-normal point maxima developed in Run 1. Passchier (1984) has also measured similar fabrics. These fabrics are consistent with those predicted by this model, but this comparison, and the ones which follow, do not in themselves demonstrate the validity of the model.

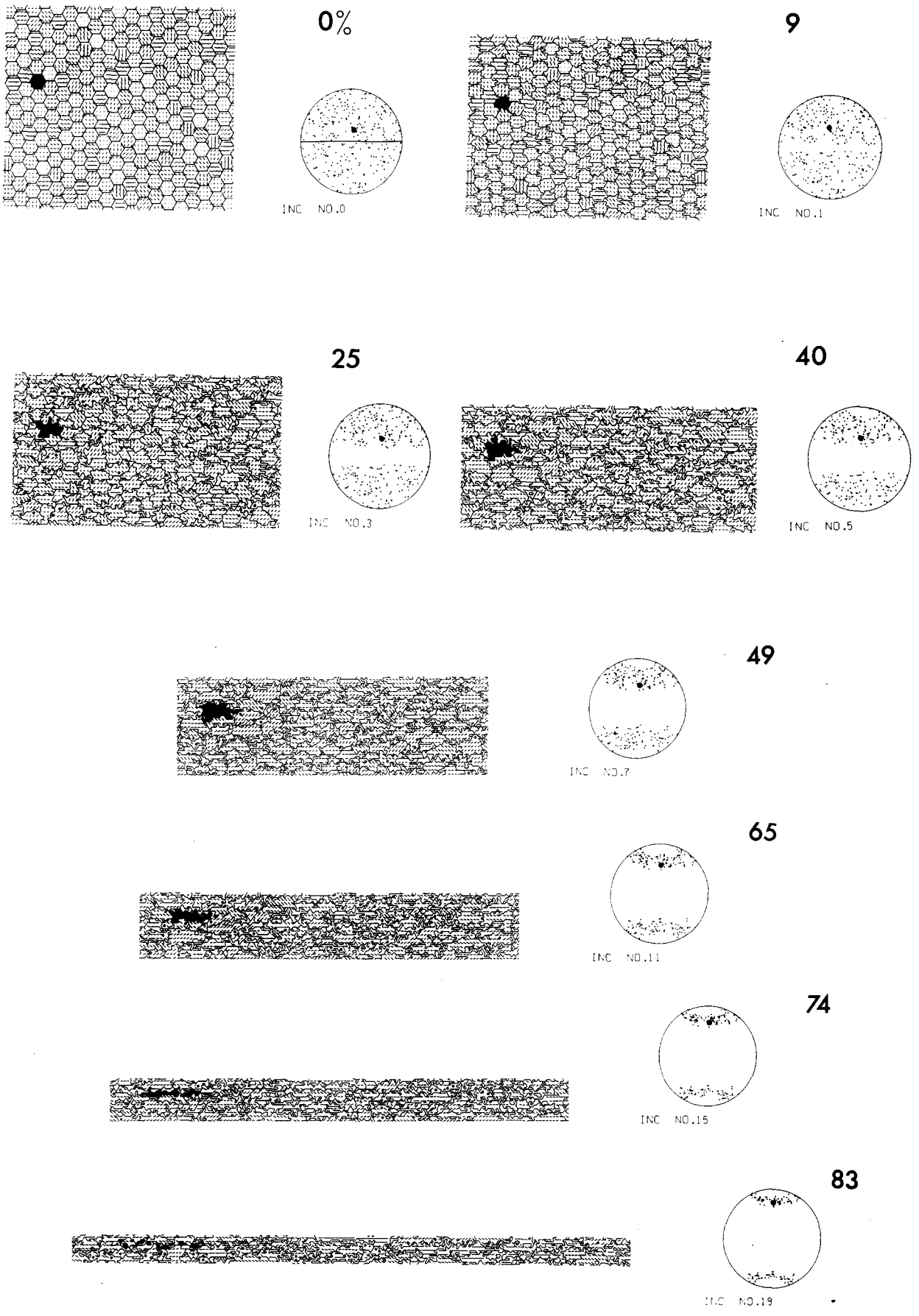

Fig. 7. Run 5: all parameters and details of the figure are as for Run 1, except that the deformation geometry is axisymmetric flattening, and thus strains shown are per cent shortening.

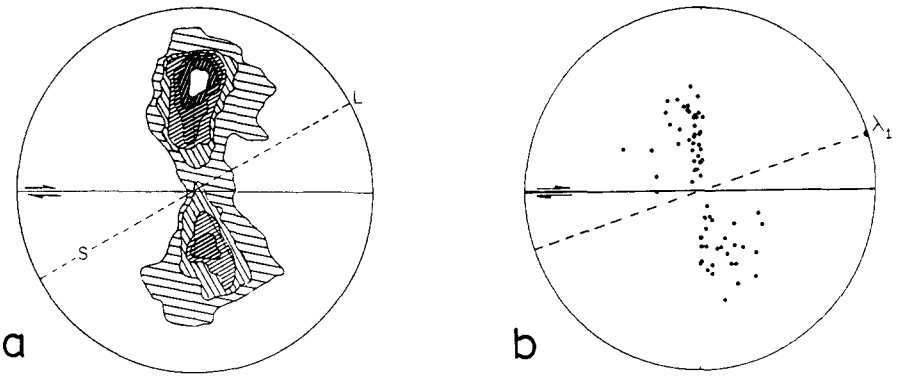

Fig. 8. Comparison of *c*-axis fabrics with double maxima close to the shear plane in simple shear. (a) Natural example from a quartzite shear zone (after Brunel 1980); *S* is foliation, *L* is lineation. (b) Run 2, shear strain = 2.85. Lower-hemisphere equal-area projections.

Sander (1950) stated that the positions of point maxima cannot be simply interpreted as being the result of single-slip deformation. These simulations seem to bear this out. Bouchez & Pêcher (1981) suggest that point maxima in similar positions to those seen at a shear strain of 2.85 in Run 2 may be the result of dominant rhomb slip, and certainly these grains are now well oriented for rhomb ⟨*a*⟩ slip. However this model suggests that the coupling of multiple slip and orientation-dependent grain boundary migration can also produce point maxima. The double maxima of Run 2 bear a remarkable similarity to a fabric measured by Brunel (1980) from a quartzite shear zone in the Himalayas (Fig. 8). Double maxima of this type have also been measured in shear zones by Eisbacher (1970), Hara *et al.* (1973), Carreras *et al.* (1977) and Passchier (1982).

In Run 2, the two-maxima fabric was seen to contract to a single maximum, parallel to the finite λ_2, or *Y* direction. Quartz *c*-axis fabrics of this type, often referred to as *Y* maxima (Fig. 9), are a commonly observed quartz fabric in shear zones (Eisbacher 1970, Hara *et al.* 1973, Bouchez 1977, Burg *et al.* 1981, White *et al.* 1982). Behrmann (1985) has observed that grains oriented with their *c*-axes near λ_2 have lower numbers of subgrains, which may be an indication that grains in this orientation have lower levels of stored energy.

Fabric evolution

It is frequently assumed that traverses across strain gradients reveal the history of the fabric developed at the highest strains (Bouchez 1977). This is not necessarily true (Means 1976); however if this assumption is made, the *c*-axis patterns described by Simpson (1980) could be interpreted as recording the interaction of recrystallization and lattice rotations. Figure 10(a) shows three quartz *c*-axis fabrics sequentially sampled across an orthogneiss shear zone from the Maggia Nappe, Switzerland. The sequence can be interpreted as evolving from a rough Type I girdle into a single point maximum perpendicular to the shear zone boundaries. In the light of Run 4 (Fig. 10b) this sequence could be interpreted as being the result of a relatively slow rate of recrystallization. This allowed the formation of a girdle before its gradual contraction to a point maximum due to basal-plane controlled variations in the stored energy of deformation.

Ice deformed in simple shear, either experimentally (Kamb 1972, Bouchez & Duval 1982) or naturally (Hudleston 1980), typically develops *c*-axis fabrics with two point maxima (Fig. 11a). The stronger maximum is perpendicular to the shear zone boundaries, although frequently about 5° away from the true perpendicular.

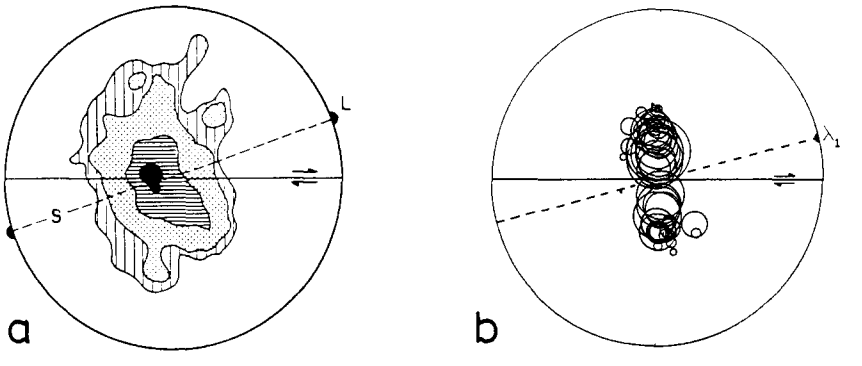

Fig. 9. Comparison of *c*-axis fabrics with *Y* maximum in simple shear. (a) Natural example (after Burg *et al.* 1981); *S* is foliation, *L* is lineation. (b) Run 2, shear strain = 3.61. Lower-hemisphere equal-area projections.

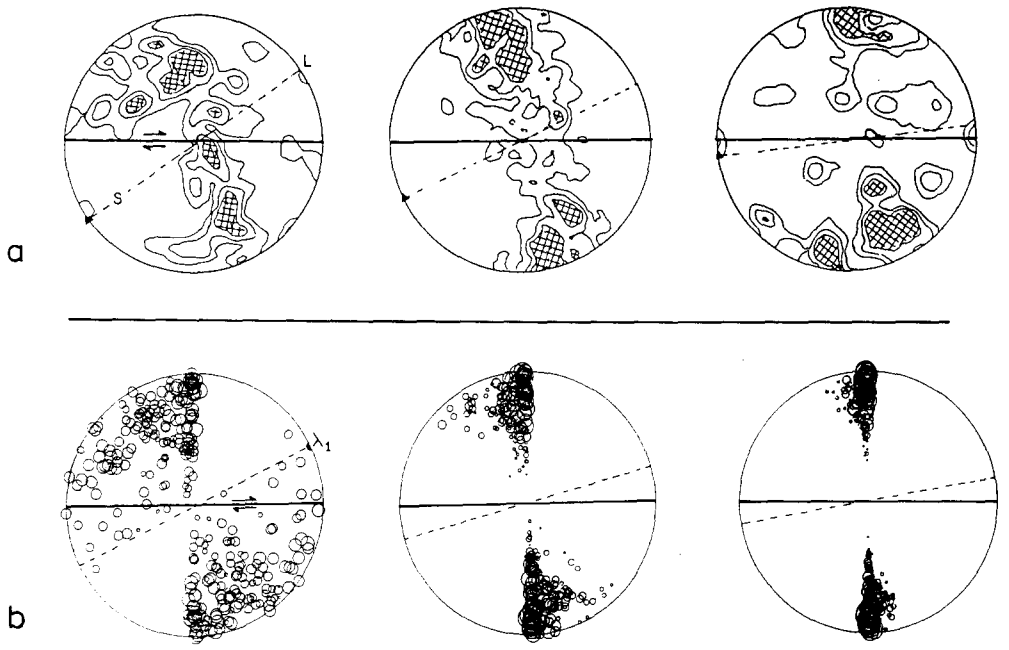

Fig. 10. Comparison of *c*-axis fabric sequences in simple shear showing the contraction of a girdle perpendicular to the shear plane into a point maximum. (a) Natural example at shear strains of 0.6, 1.6 and 6.3 (after Simpson 1980); *S* is foliation, *L* is lineation. (b) Run 4, shear strain = 1.7, 3.61 and 5.51. Lower-hemisphere equal-area projections.

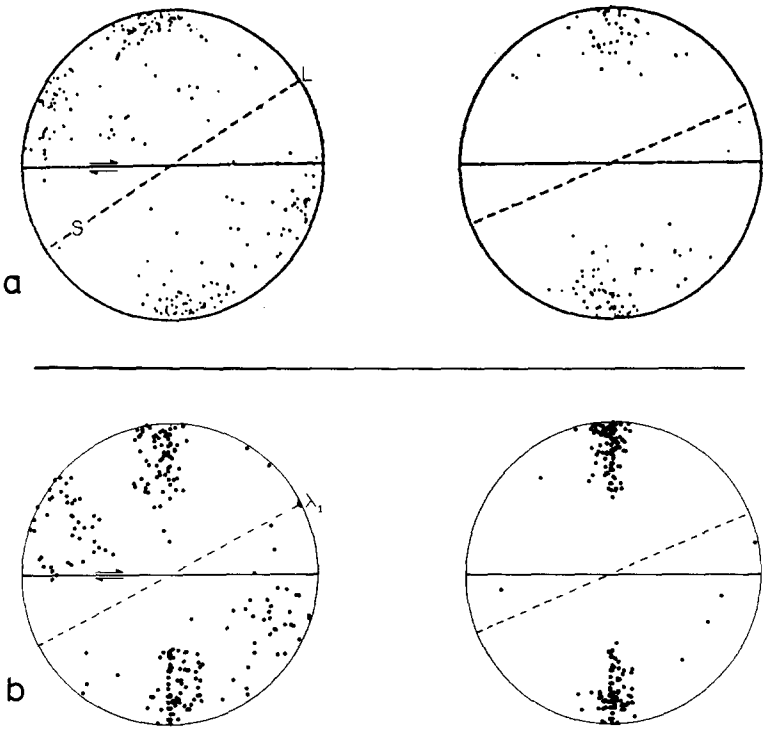

Fig. 11. Comparison of *c*-axis fabric sequences in simple shear showing a two maxima fabric that with increasing strain evolves into a single maximum perpendicular to the shear plane. (a) Experimental example in ice at shear strains of 0.95 and 2.0 (after Bouchez & Duval 1982); *S* is foliation, *L* is lineation. (b) Run 3, shear strains = 1.33 and 2.09. Lower-hemisphere equal-area projections.

The weaker maximum lies about 20° away from the shear plane. With increasing strain, the weaker maximum disappears, leaving a single point maximum. The same sequence can be seen in Run 3 (Fig. 11b), which suggests that Kamb's (1972) interpretation of this sequence as having resulted from the coupling of recrystallization and lattice rotations may be correct.

The axisymmetric flattening simulation suggests that small circle girdles may form as the result of the competition between grain boundary migration and lattice rotations, as suggested by Hooke & Hudleston (1981). The girdle in this simulation contracts with progressive strain towards a point maximum. The experimental deformation of quartzites in axisymmetric flattening by Tullis *et al.* (1973) produced point maxima in lower temperature, higher strain-rate runs without recrystallization. At higher temperatures and lower strain rates, the samples exhibit a stress drop, often associated with the onset of recrystallization (Gottstein 1983), and small circle girdles of *c*-axes were observed. The opening angle of these girdles increased with increasing temperature for the same strain. This could be accounted for by the increased mobility of grain boundaries at higher temperatures, which would result in *c*-axis girdles closer to the girdle of low stored-energy orientations at 45° to σ_1. TBH theory also predicts a change in girdle angle with temperature, if a lower critical resolved shear stress for prism ⟨*a*⟩ slip is associated with this temperature change.

Hooke & Hudleston (1981) have measured small-circle girdle angles in naturally deformed ice from the Barnes ice cap, and show a trend of decreasing girdle angle with increasing strain. Marjoribanks (1976) reported a similar correlation from naturally deformed quartzites; in this case, however, there is very little evidence for recrystallization. In the experiments of Tullis *et al.* (1973) there is also some evidence that the small-circle girdles contract with increasing strain (Fig. 12), which is consistent with the simulation results.

Grain-shape fabrics

The grain-shape foliations in the simulations without subgrain formation either track the maximum finite extension orientation, or lag slightly behind it. With subgrain formation, the foliation lags much further behind. The combination of large elongate grains and smaller rounder grains that develop in this case are comparable to many natural fabrics from fault zones (Weathers *et al.* 1979).

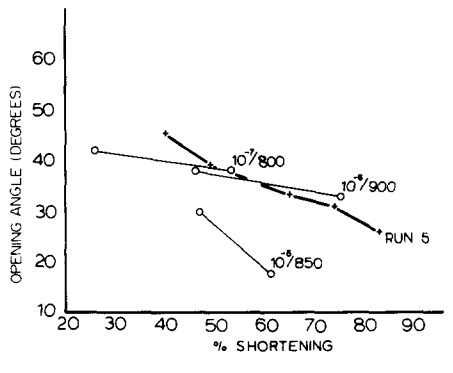

Fig. 12. Change in opening angle of small-circle girdles in axisymmetric flattening. Circles are for experimentally deformed quartzites (unpublished data of J. Tullis personal communication 1986), crosses for Run 5. The numbers next to the quartzite data refer to the imposed strain rate (s^{-1}) and temperature (°C) for each pair of experiments.

These simulations cannot account for the observation of oblique quartz foliations at very high angles to the shear plane (Garcia Celma 1982), nor for the strong grain boundary alignments observed by Schmid *et al.* (1987) in experimentally deformed calcite and by Koenemann (1985) in naturally deformed quartzites.

The simple shear simulations tend to form strong point-maximum *c*-axis fabrics at high strains, when orientation-dependent variations in the stored energy of deformation are inevitably low. As a result, other weak orientation-dependent effects may become relatively more important (Abruzzese & Lucke 1986). There may be a case for a crystallographically-controlled surface energy driving force for grain boundary migration, to produce, for example, the domainal fabrics of Garcia Celma (1982), in which grain boundaries are aligned perpendicular to the average basal plane orientation of each domain. A correlation between grain shapes and crystal orientations has also been reported by Ohtomo & Wakahama (1983) in a naturally deformed ice which had a strong crystallographic fabric.

Grain size distributions

Experimental evidence suggests that grain size in recrystallizing rocks can be correlated with the flow stress, so it is perhaps surprising that large variations in grain size are seen among the various simulation runs. Significant grain size differences result not only from the different recrystallization processes (grain boundary migration with or without subgrain formation), but also from different grain boundary mobilities, and even from strain geometries. It remains to be seen whether these differences are observed in real polycrystals.

It is a common observation that deformation leads to grain size reduction, although at higher temperatures grain growth may occur. These simulations produced both types of behaviour, although all of the runs started out with a grain size reduction. The grain-size minimum of Runs 1 and 2 has been observed in experimentally deformed ice by Wilson & Russell-Head (1982). They also observed faster fabric development in the finer grained ices, which may indicate that grain boundary migration is a major crystallographic fabric modifying process in ice, since a reduction in grain size is geometrically equivalent to an increase in mobility (ignoring rheological differences which may result). This conclusion is supported by the sharp crystallographic fabrics measured in ice by Kamb (1972) at shear strains far too low ($\gamma = 0.29$) to be accounted for by any slip-induced lattice rotation model.

Comparison of Runs 1 and 4 suggests that the lower rates of migration actually lead to smaller grain sizes,

although none of the runs reached steady state conditions. Although they have not been analysed in detail, grain size distributions appear to be different for different runs, and certainly evolve with time for a single run.

CONCLUSIONS

(1) These simulations suggest that the coupling of orientation-dependent grain boundary migration with lattice rotations due to dislocation glide can produce crystallographic fabrics that are significantly different from those resulting from dislocation glide alone, and many of the *c*-axis fabrics predicted by this simulation have counterparts in naturally and experimentally deformed quartzite and ice.

(2) In the extreme, the effects of grain boundary migration on crystallographic fabrics can be quite pronounced without dramatic modification of the grain-shape fabric.

(3) As distinct from the predictions of Taylor–Bishop–Hill theory, progressive deformation may produce different fabrics, even when the same straining geometry and lattice rotations are assumed, and these fabrics may evolve significantly with increasing strain.

(4) The formation and positions of *c*-axis point maxima do not necessarily reflect the results of the activity of single slip systems.

(5) The simulation predicts that there may be measurable differences in the behaviour of recrystallizing polycrystals when subjected to axisymmetric flattening and simple shear, quite apart from the direct effects of the differences in strain geometry.

(6) The simulation can produce grain-shape fabrics oblique to the finite strain axes; however it cannot account for strong patterns of preferred grain boundary alignments at high angles to the shear plane.

Acknowledgements—I would like to thank Win Means for his constant encouragement during this study, and for suggesting many improvements to the model and its description. Jan Tullis, Brian Bayly, Janos Urai and an anonymous reviewer also read versions of this work and made many helpful comments. Gordon Lister provided me with the lattice rotation figures for simple shear, which were at that time unpublished. Jan Tullis provided me with new *c*-axis fabric data, and I am most grateful for her permission to use it. This work was carried out with the help of NSF grant EAR 8306166 to Win Means.

REFERENCES

Abruzzese, G. & Lucke, K. 1986. A theory of texture controlled grain growth. I. Derivation and general discussion of the model. *Acta metall.* **34**, 905–914.

Behrmann, J. H. 1985. Crystal plasticity and super-plasticity in quartzite: a natural example. *Tectonophysics* **115**, 101–129.

Bouchez, J. L. 1977. Plastic deformation of quartzites at low temperature in an area of a natural strain gradient. *Tectonophysics* **39**, 25–50.

Bouchez, J. L. & Duval, P. 1982. The fabric of polycrystalline ice deformed in simple shear: experiments in torsion, natural deformation and geometric interpretation. *Textures Microstruct.* **5**, 171–190.

Bouchez, J. L., Lister, G. S. & Nicolas, A. 1983. Fabric asymmetry and shear sense in movement zones. *Geol. Rdsch.* **72**, 401–419.

Bouchez, J. L. & Pêcher, A. 1981. The Himalayan main central thrust pile and its quartz-rich tectonites in central Nepal. *Tectonophysics* **78**, 23–50.

Brunel, M. 1980. Quartz fabrics in shear-zone mylonites: evidence for a major imprint due to late strain increments. *Tectonophysics* **64**, T33–T44.

Burg, J. P., Iglesias, M., Laurent, Ph., Matte, Ph. & Ribeiro, A. 1981. Variscan intracontinental deformation: the Coimbra–Cordoba shear zone (S.W. Iberian Peninsula). *Tectonophysics* **78**, 161–177.

Carreras, J., Estrada, A. & White, S. H. 1977. The effects of folding on the c-axis fabrics of a quartz mylonite. *Tectonophysics* **39**, 15–42.

Duval, P. 1981. Creep and fabrics of polycrystalline ice under shear and compression. *J. Glaciol.* **27**, 129–140.

Eisbacher, G. H. 1970. Deformation mechanics of mylonitic rocks and fractured granites in Cobequid Mountains, Nova Scotia, Canada. *Bull. geol. Soc. Am.* **81**, 2009–2020.

Etchecopar, A. 1977. A plane kinematic model of progressive deformation in a polycrystalline aggregate. *Tectonophysics* **39**, 121–139.

Garcia Celma, A. 1982. Domainal and fabric heterogeneities in the Cap de Creus mylonites. *J. Struct. Geol.* **4**, 443–455.

Gottstein, G. 1983. Dynamic recrystallization of Cu single crystals during tensile deformation in creep. *Met. Sci.* **17**, 1142–1173.

Hara, I., Takeda, K. & Kimura, T. 1973. Preferred lattice orientation of quartz in shear deformation. *J. Sci. Hiroshima Univ.*, Series **C7**, 1–10.

Hooke, R. Le B. & Hudleston, P. J. 1981. Ice fabrics from a borehole at the top of the south dome, Barnes Ice Cap, Baffin Island. *Bull. geol. Soc. Am.* **92**, 274–281.

Hudleston, P. J. 1980. The progressive development of inhomogeneous shear and crystallographic fabric in glacial ice. *J. Struct. Geol.* **2**, 189–196.

Jessell, M. W. 1986. Grain boundary migration and fabric development in experimentally deformed octachloropropane. *J. Struct. Geol.* **8**, 527–542.

Jessell, M. W. 1988. Simulation of fabric development in recrystallizing aggregates—I. Description of the model. *J. Struct. Geol.* **10**, 771–778.

Kamb, W. B. 1972. Experimental recrystallization of ice under stress. *Am. Geophys. Un. Geophys. Monogr.* **16**, 211–241.

Koenemann, F. 1985. Progressive deformation textures in granite from incipient to advanced strains. (Abs.) *Geol. Soc. Am. Abs. w. Prog.* **17**, 632.

Lister, G. S., Paterson, M. S. & Hobbs, B. E. 1978. The simulation of fabric development during plastic deformation and its application to quartzite: the model. *Tectonophysics* **45**, 107–158.

Marjoribanks, R. W. 1976. The relation between microfabric and strain in a progressively deformed quartzite sequence from central Australia. *Tectonophysics* **32**, 269–293.

Means, W. D. 1976. *Stress and Strain*. Springer-Verlag, New York.

Ohtomo, M. & Wakahama, G. 1983. Correlation between crystallographic axes and the shape of a single crystal in glaciers. *J. Glaciol.* **29**, 498–504.

Passchier, C. W. 1982. Mylonitic deformation in the Saint Barthelemy Massif, French Pyrenees, with emphasis on the genetic relationship between ultramylonites and pseudotachylite. Unpublished Ph.D. thesis, University of Amsterdam, The Netherlands.

Passchier, C. W. 1984. The reliability of asymmetric *c*-axis fabrics of quartz for determining the sense of vorticity. *Tectonophysics* **99**, T9–T18.

Price, G. P. 1985. Preferred orientation in quartzites. In: *Preferred Orientation in Deformed Metals and Rocks* (edited by H.-R. Wenk). Academic Press, New York.

Sander, B. 1950. *Einführung in die Gefügekunde der Geologischen Körper*, Vol. 2. Springer, Vienna.

Schmid, S. M. & Casey, M. 1986. Complete fabric analysis of some commonly observed quartz *c*-axis patterns. *Am. Geophys. Un. Geophys. Monogr.* **36**, 263–286.

Schmid, S. M., Panozzo, R. & Bauer, S. 1987. Special Research Paper. Simple shear experiments on calcite rocks: rheology and microfabric. *J. Struct. Geol.* **9**, 747–778.

Simpson, C. 1980. Oblique girdle orientations of quartz *c*-axes from a shear zone in the basement core of the Maggia Nappe, Ticino, Switzerland. *J. Struct. Geol.* **2**, 243–247.

Tullis, J., Christie, J. M. & Griggs, D. T. 1973. Microstructure and preferred orientation of experimentally deformed quartzites. *Bull. geol. Soc. Am.* **84**, 297–314.

Urai, J. L. 1983. Deformation of wet salt rocks. Unpublished Ph.D. thesis, University of Utrecht, The Netherlands.

Urai, J. L. & Humphreys, F. J. 1981. The development of shear zones in polycrystalline camphor. *Tectonophysics* **78**, 677–685.

Urai, J. L., Means, W. D. & Lister, G. S. 1986. Dynamic recrystallisation of minerals. *Am. Geophys. Un. Geophys. Monogr.* **36**, 161–199.

Weathers, M. S., Bird, J. M., Cooper, R. F. & Kohlstedt, D. L. 1979. Differential stress determination from deformation-induced microstructures of the Moine Thrust Zone. *J. geophys. Res.* **84**, 7495–7509.

White, S. H., Evans, D. J. & Zhoung, D.-L. 1982. Fault rocks of the Moine Thrust Zone: microstructures and textures of selected mylonites. *Textures Microstruct.* **5**, 33–61.

Wilson, C. J. L. 1973. The prograde microfabric in a deformed quartzite sequence, Mount Isa, Australia. *Tectonophysics* **19**, 39–81.

Wilson, C. J. L. & Russell-Head, D. S. 1982. Steady-state preferred orientation of ice deformed in plane strain at −1°C. *J. Glaciol.* **28**, 145–160.